Effects of Bath Composition and Current Density on the Electrodeposition Behavior of Fe–Ni Invar Alloy

Na-Young Kang[1] · Jae-Ho Lee[1]

Abstract

Fe–Ni invar alloy (Fe 64–Ni 36 wt%) has a very low coefficient of thermal expansion (CTE) than any other metals. For this reason, it has been used as fine metal mask (FMM) in RGB patterning of OLED manufacture process. However, as the resolution of OLED display is getting higher, the thickness of FMM is getting thinner and then the conventional extruded invar sheet cannot be used directly. The electrodeposition of invar can be the alternative for fabrication of thin FMM. In this study, the Fe–Ni alloy were electrodeposited varying bath compositions and current density. Also, the effects of ferric ion (Fe^{3+}), produced during electrodeposition on inert anode, on the behavior of deposition were investigated. Finally, the Fe–Ni alloy with 36–40 wt% Ni were obtained at 50 mA/cm^2 in 0.30 M Fe^{2+} bath. The back side and front side composition of the deposits were analyzed to evaluate the composition uniformity of the Fe–Ni alloys. Generally, the Fe content of back side of the deposits were higher than that of front side.

Graphical Abstract
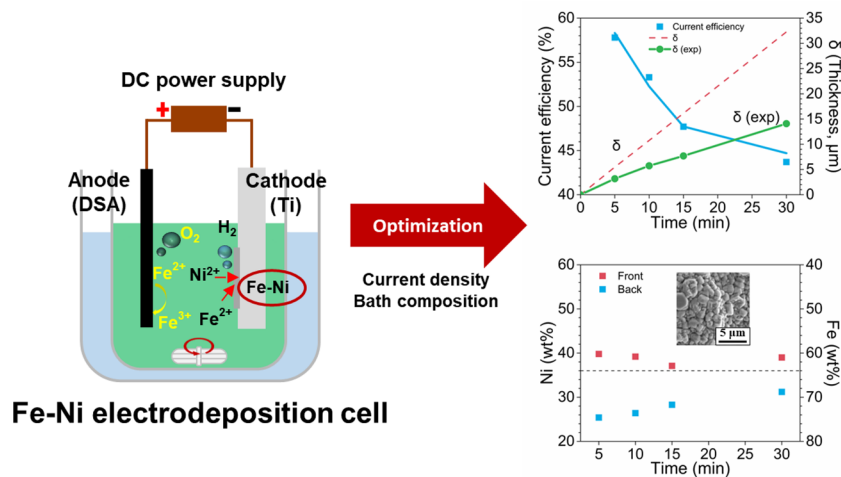
1 Introduction

Fe–Ni alloy with Fe 64–36 wt% Ni, commercially known as invar, has a low thermal expansion coefficient (CTE) than any other metals [1]. Based on its dimensional stability,

Fe–Ni invar has been used as the materials of fine metal mask(FMM), a key component in RGB patterning of organic light-emitting diode (OLED) display, to avoid distortion of

✉ Jae-Ho Lee
  jhlee@hongik.ac.kr

1 Department of Materials Science and Engineering, Hongik University, Seoul 04066, Republic of Korea
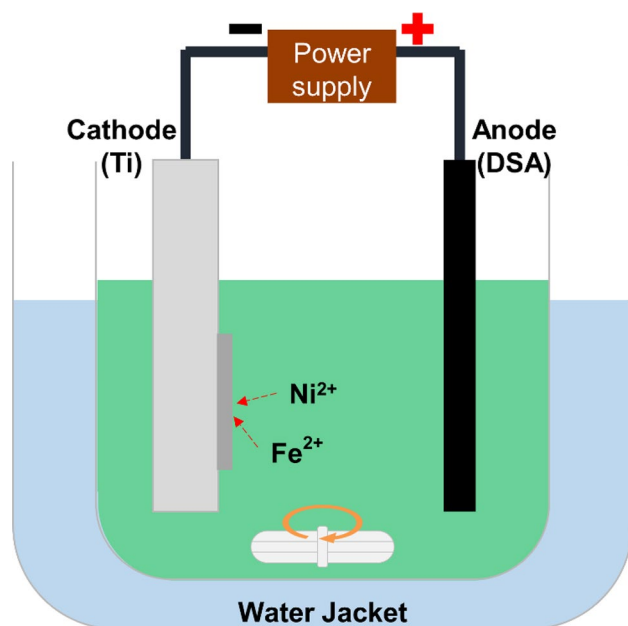
Fig. 1 Schematic image of the Fe–Ni electrodeposition cell

patterns during evaporation process at high temperature [2–4].

Nowadays, commercialized FMM has been produced by wet etching process of invar film with over 20 µm in thickness made by rolling process. However, it is impossible to get higher resolution than QHD with extruded invar thickness [5, 6], therefore, several studies about alternative technology for higher resolution have been conducted. Electrodeposition is considered as one of the methods to make thinner FMM of 15 µm or less, whose resolution is higher than QHD by relatively simple equipment and process, compared to other technologies [7].

However, the properties of electrodeposited Fe–Ni film, such as composition, microstructure, surface morphology, are significantly influenced by various process conditions (bath composition, current density, temperature, pH, additive and etc.) [8, 9, 11]. For this reason, it is important to understand the effects of each variable on the deposits in order to apply electrodeposition to mass production of high resolution FMM. In this study, the electrodeposition of Fe–Ni alloy was conducted at various bath composition of ferrous ion (Fe^{2+}) and current density. Also, ferric ion (Fe^{3+}) was added to bath to observe the effect of ferric ion on Fe–Ni electrodeposition behavior. Finally, Fe–Ni films close to invar composition were obtained and the uniformity of deposited was evaluated.

2 Experimental Details

In this study, Fe–Ni alloy electrodeposition was conducted in sulfate–chloride bath using dimensionally stabilized anode (DSA) as anode, Ti plate with exposed area of 2 cm × 2 cm as cathode, which cleaned with 10 wt% NaOH solution and 10 wt% H_2SO_4 solution in ultrasonic cleaner before electrodeposition. The electrolyte consisted of 0.95 M nickel(II) sulfate, 0.17 M nickel(II) chloride, 0.25–0.4 M iron(II) sulfate, 0.5 M boric acid, 0.05 M malonic acid and 2 g/L sodium saccharin. Iron(III) sulfate was added for investigation of Fe^{3+} effects. The pH of bath was adjusted to 2.3 with 20 wt% NaOH solution and 10 wt% H_2SO_4 solution. The temperature of bath was maintained at 50 °C in water jacket and bath was stirred with 300 rpm using 28 mm magnetic bar. The schematic diagram of the electrodeposition cell is shown in Fig. 1. The current density was varied from 10 to 200 mA/cm², and deposition time was adjusted with each current density to maintain total charge of 192 C. The Fe–Ni deposits was cleaned with distilled water and dried after electrodeposition.

The compositions of the Fe–Ni deposits were analyzed using energy dispersive X-ray spectroscopy (EDS). Field emission scanning electron microscope (FESEM) was used for analysis of surface morphology and thickness for calculation of current efficiency. Potentiodynamic polarization was conducted at three electrode system, consisting of Ag/AgCl electrode as reference electrode, Ti plate as working electrode, and DSA as counter electrode. The scan rate was 5 mV/s and operating voltage range was from 0.05 V (vs open circuit voltage, OCV) to − 1.8 V (vs Ag/AgCl). Residual stress of deposits were analyzed using deposit stress analyzer model 683, and the condition of temperature and total charge for the electrodeposition of strip were room temperature (RT) and 45 C, respectively.
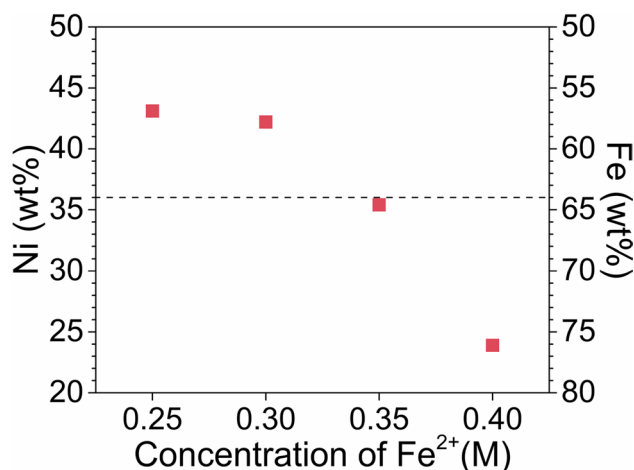

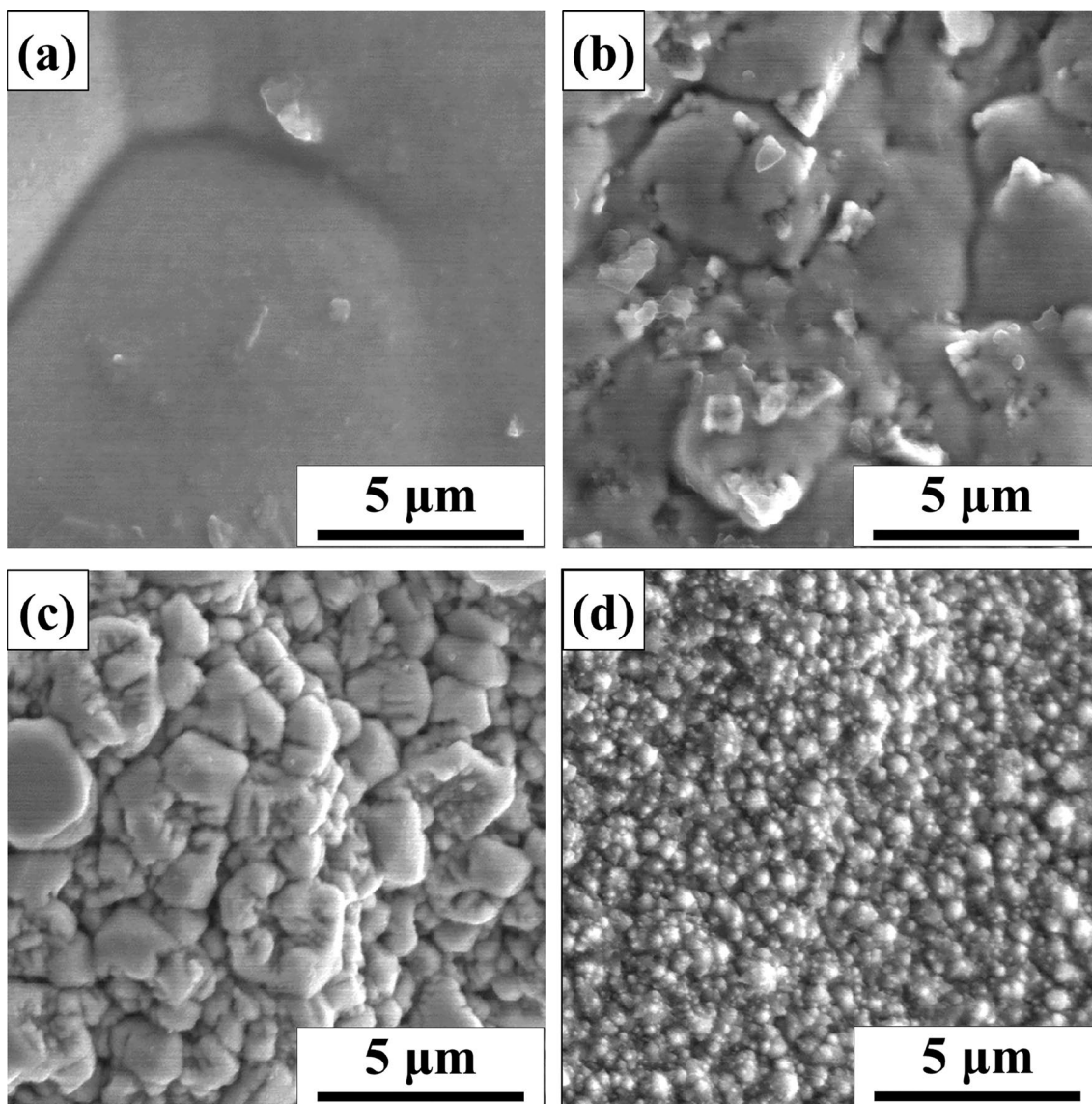**Fig. 2** Composition of the deposits vs Concentration of iron(II) sulfate (current density (i) = 50 mA/cm²)

Fig. 3 Surface morphology of Fe–Ni electrodeposits at various concentration of Fe^{2+} (**a** 0.25 M, **b** 0.30 M, **c** 0.35 M, **d** 0.40 M)

Table 1 Standard reduction potential(E^o) of possible redox reactions in the Fe–Ni electrodeposition cell [12]

Reaction		E^o (V vs. standard hydrogen electrode)
Anodic	$2H_2O = O_2 + 4H^+ + 4e^-$	1.23
	$Fe^{2+} = Fe^{3+} + e^-$	0.77
Cathodic	$Fe^{3+} + e^- = Fe^{2+}$	0.77
	$2H^+ + 2e^- = H_2$	0.00
	$Ni^{2+} + 2e^- = Ni$	−0.26
	$Fe^{2+} + 2e^- = Fe$	−0.44

3 Results and Discussion

Figure 2 shows the composition of the deposits from bath with 0.25, 0.30, 0.35, 0.40 M iron(II) sulfate ($FeSO_4$). For all bath conditions, the Fe content of deposits were higher than Fe content of the baths. It means that Fe–Ni alloy was electrodeposited anomalously, as active Fe preferentially deposited than Ni [10, 11]. The deposits became Fe-richer as the concentration of Fe^{2+} increased. In 0.35 M Fe^{2+} bath, the Fe–Ni film with 35.4 wt% Ni, similar to invar composition, was obtained. The surface morphologies of the deposits are shown in Fig. 3. The morphology of deposits at low Fe^{2+} concentration showed the bright surface, however the surface morphology was changed to rougher and lost the
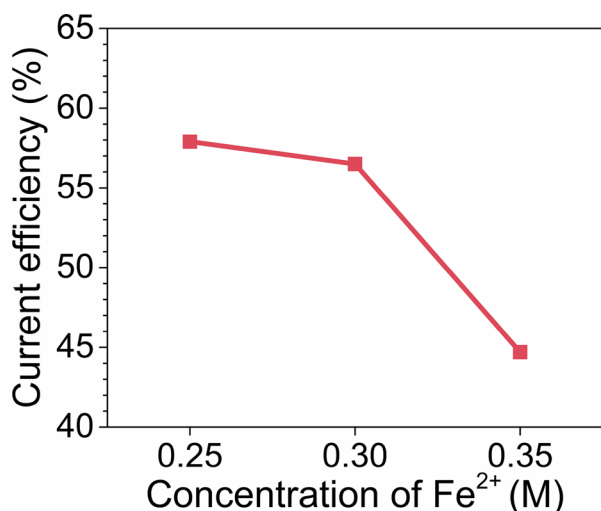
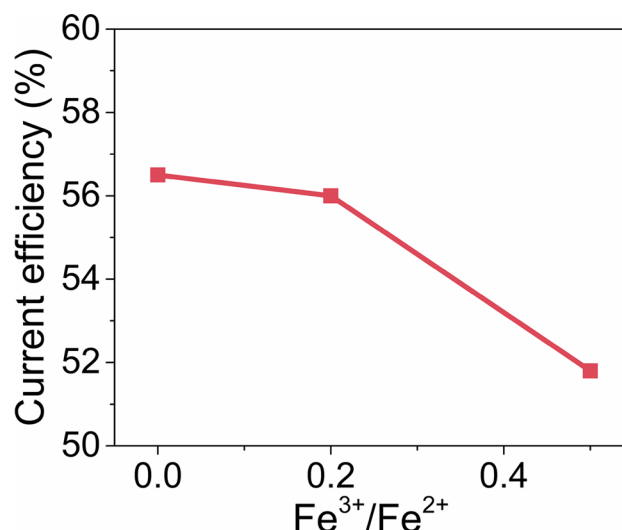**Fig. 4** Current efficiency at various concentration of Fe^{2+}
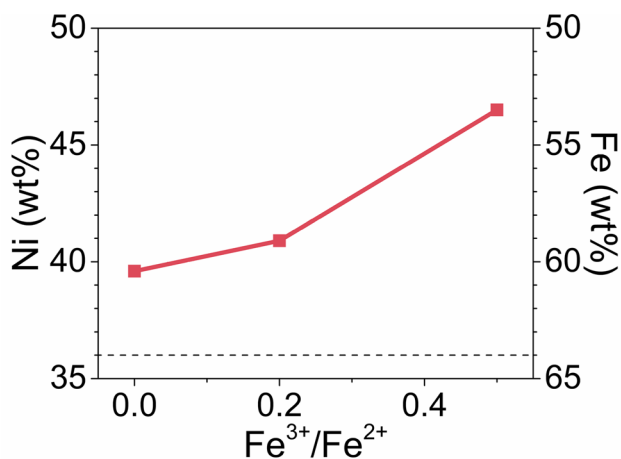

Fig. 6 Current efficiency at various Fe^{3+}/Fe^{2+} conditions

Fig. 5 Composition of deposits from different Fe^{3+}/Fe^{2+} bath

Fig. 7 Composition of deposits at various current density ($[Fe^{2+}] = 0.35$ M)

brightness as the Fe^{2+} concentration increased. The current efficiency of each bath was calculated from the thickness of deposits. As shown in Fig. 4, the current efficiency was decreased as the concentration of Fe^{2+} became higher, from 57.9% at 0.25 M to 44.7% at 0.35 M Fe^{2+}. It means that competing reactions were occurred during Fe–Ni alloy electrodeposition, such as hydrogen evolution reaction and Fe^{2+}/Fe^{3+} redox reactions. Standard reduction potential(E°) of possible redox reactions in the Fe–Ni electrodeposition cell are listed in Table 1 [12].

To investigate the effect of Fe^{3+} in bath, Fe–Ni electrodeposition was conducted in the modified bath containing 0, 0.05, 0.10 M iron(III) sulfate, which the sum of Fe^{2+} and Fe^{3+} was kept at 0.30 M. As shown in Fig. 5, the Fe content of deposits from the bath with higher Fe^{3+} content was lower. In addition, the current efficiency was reduced from 56.5 to 51.8% as the concentration of Fe^{3+} increased (Fig. 6).

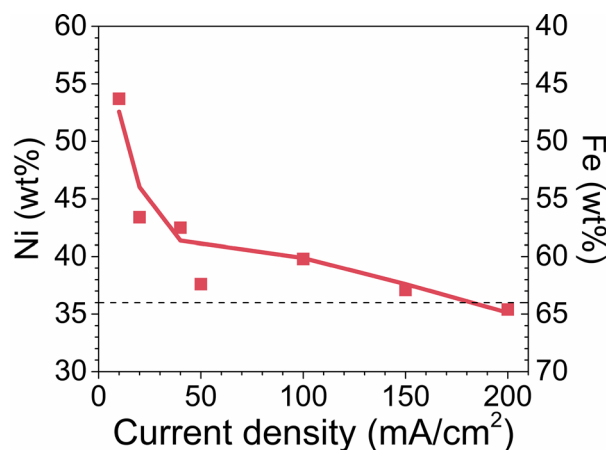It means that Fe^{3+} produced on the DSA suppress Fe reduction on the cathode due to consumption of charge for Fe^{2+}/Fe^{3+} redox reactions.

Figure 7 shows the composition of deposit from 0.35 M Fe^{2+} bath depending on current density. The composition change in the high current density region over 50 mA/cm² was negligible compared to that in the low current density region from 10 to 50 mA/cm². It is due to the current density reached the diffusion controlled region as shown in the cathodic polarization plot (Fig. 8), where charge transfer rate was so fast that total reaction rate is determined by diffusion of reactants [13, 14]. Figures 9 and 10 show the residual stress and current efficiency at various current density respectively. All deposits showed the tensile stress and it was increased with current density. The current efficiency
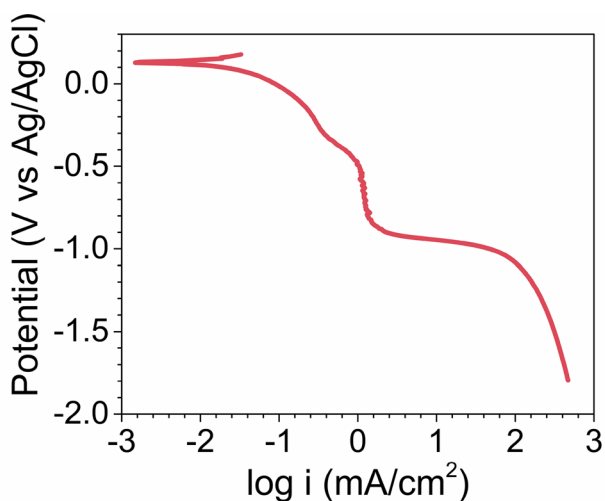
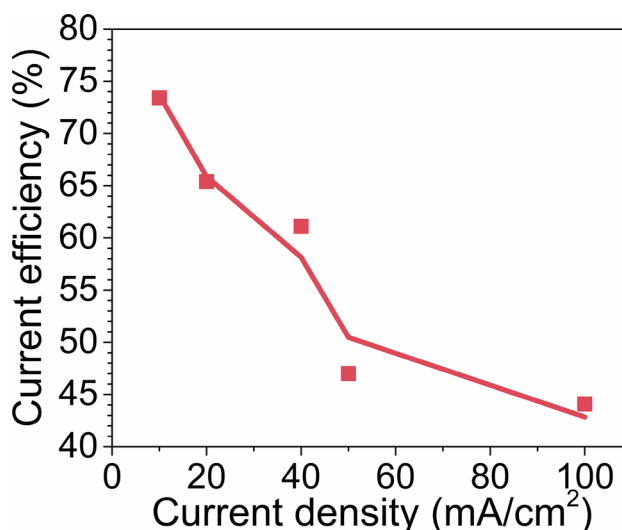**Fig. 8** Polarization plots in 0.35 M iron(II) sulfate bath

Fig. 9 Residual stress at various current efficiency ($[Fe^{2+}] = 0.35$ M, T = RT)

Fig. 10 Current efficiency of deposits with varying current density
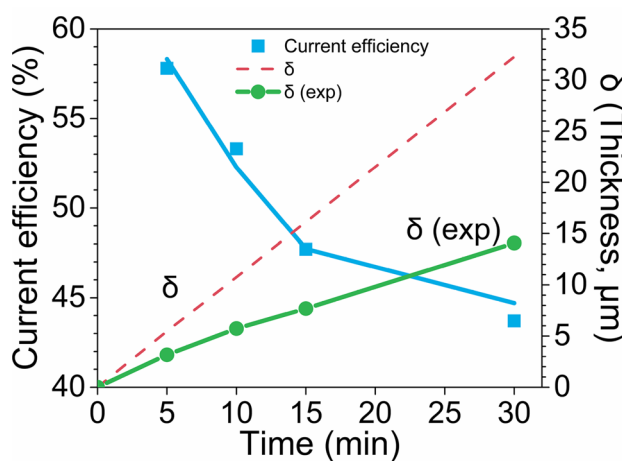

Fig. 11 Current efficiency and thickness of deposits vs deposition time (i = 50 mA/cm², $[Fe^{2+}] = 0.30$ M)

was decreased from 73% at 10 mA/cm² to 44% at 100 mA/cm². As the current density became higher, the rate of charge transfer for reduction of proton in bath get faster whereas the rate of reduction of metal ions became diffusion-controlled. As the results, more hydrogen gases were evolved on deposit, leading to low efficiency and high tensile stress [15, 16].

The composition range of electrodeposited Fe–Ni, which is showing minimum CTE, was 36–41 wt%, on the other hand the pyrometallurgically produced one was about 36 wt% Ni [17]. For this reason, the Fe–Ni alloy was electrodeposited at 50 mA/cm² in 0.30 M Fe²⁺ bath for 5, 10, 15, 30 min. Figure 11 shows thickness of deposits(δ) and

current efficiency depending on deposition duration. For all conditions, the thickness of deposits were thinner than theoretical thickness($δ_{exp}$) and the difference between them became larger, leading to decrease in current efficiency. The results of composition analysis are shown in Fig. 12. The Ni contents of the front side of deposits were 36–40 wt% Ni regardless of deposition time, however, the back side of deposits contain more Fe than front side at all conditions. The Fe–Ni alloy was electrodeposited anomalously, and the commonly reported mechanism of anomalous codeposition was shown below [18–21].
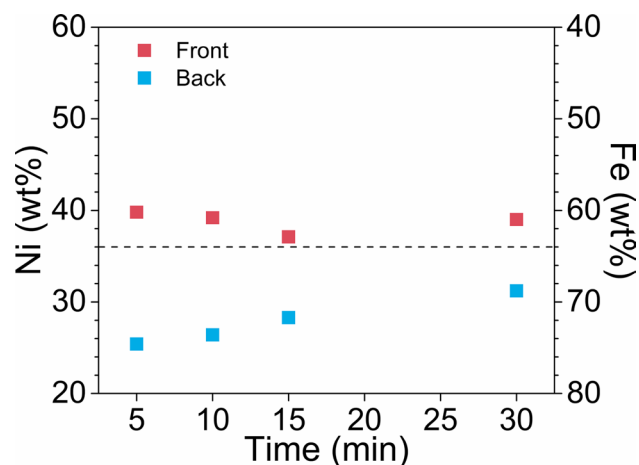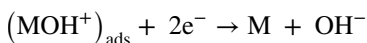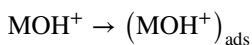
$$2H_2O + 2e^- \rightarrow H_2 + 2OH^-$$

$$M^{2+} + OH^- \rightarrow MOH^+$$
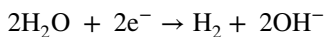
Fig. 12 Composition of front and back side of deposits vs. deposition time

$$MOH^+ \rightarrow \left(MOH^+\right)_{ads}$$

$$\left(MOH^+\right)_{ads} + 2e^- \rightarrow M + OH^-$$

In these equation, M is iron group metal (Fe, Ni, Co) and the adsorption ability of each metal monohydroxide ion (MOH^+) is strong in order of Fe, Co, Ni [22]. Thus $Fe(OH)^+$, preferentially adsorbed on the cathode, inhibited adsorption of $Ni(OH)+$ and caused higher Fe content of the back side of deposits compared to that of the front side.

4 Conclusion

The effects of bath composition and current density on Fe–Ni electrodeposition behavior and properties of deposits were investigated. The Fe–Ni alloy films with 36–40 wt% Ni were deposited at optimized conditions. The anomalous codeposition of Fe–Ni, the preferential deposition of more active Fe, was shown in all conditions and it was profound at higher Fe^{2+} concentration and higher current density. However, the decrease in current efficiency was observed at the same time, due to Fe^{2+}/Fe^{3+} redox reaction and hydrogen evolution. For efficient and stable electrodeposition, Fe^{3+} in the bath should be controlled as low as possible and the excessively high current density should be avoided. In addition there was the difference in composition between the front and back of deposits in all deposition time. Therefore, for the application of electrodeposition to fabrication of FMM, the uniformity of deposits' properties should be secured by additional process.

Declarations

Conflict of interest The authors declare no conflicts of interest.

References

1. Wassermann, E.F.: The invar problem. J. Magn. Magn. Mater. **100**(1–3), 346–362 (1991). https://doi.org/10.1016/0304-8853(91)90828-X
2. Koden, M.: OLED Displays and Lighting. Wiley, New York (2016)
3. Choi, W., Kim, H.Y., Jeon, J.W., Chang, W.S., Cho, S.H.: Vibration-assisted femtosecond Laser drilling with controllable taper angles for AMOLED fine metal mask fabrication. Materials **10**(2), 212 (2017). https://doi.org/10.3390/ma10020212
4. Nagayama, T., Yamamoto, T., Nakamura, T., Mizutani, Y.: Fabrication of low CTE metal masks by the Invar Fe-Ni alloy electroforming process for large and fine pitch OLED displays. ECS Trans. **50**(52), 117 (2013). https://doi.org/10.1149/05052.0117ecst
5. Kim, C., Kim, K., Kwon, O., Jung, J., Park, J.K., Kim, D.H., Jung, K.: Fine metal mask material and manufacturing process for high-resolution active-matrix organic light-emitting diode displays. J. Soc. Inform. Display **28**(8), 668–679 (2020). https://doi.org/10.1002/jsid.901
6. Chen, X., Pan, T.K., Xu, W.: 76–1: invited paper: electroforming fine-metal mask for high-resolution OLED displays. SID Symp. Digest Tech. Papers **51**(1), 1128–1130 (2020). https://doi.org/10.1002/sdtp.14074
7. Li, A., Zhu, Z., Liu, Y., Hu, J.: Ultrasound-assisted electrodeposition of Fe-Ni film for OLED mask. Mater. Res. Bull. **127**, 110845 (2020). https://doi.org/10.1016/j.materresbull.2020.110845
8. Srimathi, S.N., Mayanna, S.M., Sheshadri, B.S.: Electrodeposition of binary magnetic alloys. Surface Technol. **16**(4), 277–322 (1982). https://doi.org/10.1016/0376-4583(82)90021-8
9. Lee, T.R., Chang, L., Chen, C.H.: Effect of electrolyte temperature on composition and phase structure of nanocrystalline Fe–Ni alloys prepared by direct current electrodeposition. Surf. Coat. Technol. **207**, 523–528 (2012). https://doi.org/10.1016/j.surfcoat.2012.07.069
10. Brenner, A.: Electrodeposition of Alloys : Principles and Practice, vol. I. Academic Press, Cambridge (1963)

11. Kashiwa, Y., Nagano, N., Takasu, T., Kobayashi, S., Fukuda, K., Nakano, H.: Effects of electrolyte composition and additives on the formation of invar Fe–Ni alloys with low thermal expansion electrodeposited from sulfate bath. ISIJ Int. **59**(3), 514–523 (2019). https://doi.org/10.2355/isijinternational.ISIJINT-2018-676

12. Bard, A., Parsons, R., Jordan Eds, J. Standard Potentials in Aqueous Solution, Dekker. (1985)

13. Grimmett, D.L., Schwartz, M., Nobe, K.: Pulsed electrodeposition of iron–nickel alloys. J. Electrochem. Soc. **137**(11), 3414 (1990). https://doi.org/10.1149/1.2086231

14. Andricacos, P.C., Arana, C., Tabib, J., Dukovic, J., Romankiw, L.T.: Electrodeposition of nickel–iron alloys: I. Effect of agitation. J. Electrochem. Soc. **136**(5), 1336 (1989). https://doi.org/10.1149/1.2096917

15. Armyanov, S., Sotirova-Chakarova, G.: Hydrogen desorption and internal stress in nickel coatings obtained by periodic electrodeposition. J. Electrochem. Soc. **139**(12), 3454 (1992). https://doi.org/10.1149/1.2069098

16. Dragos, O., Chiriac, H., Lupu, N., Grigoras, M., Tabakovic, I.: Anomalous codeposition of fcc NiFe nanowires with 5–55% Fe and their morphology, crystal structure and magnetic properties. J. Electrochem. Soc. **163**(3), D83 (2015). https://doi.org/10.1149/2.0771603jes

17. Park, Y.B., Kim, I.G.: The gain of low thermal expansivity via phase transition in electroformed invar. Coatings **8**(5), 169 (2018). https://doi.org/10.3390/coatings8050169

18. Hessami, S., Tobias, C.W.: A mathematical model for anomalous codeposition of nickel-iron on a rotating disk electrode. J. Electrochem. Soc. **136**(12), 3611 (1989). https://doi.org/10.1149/1.2096519

19. Yin, K.M.: Potentiostatic deposition model of iron-nickel alloys on the rotating disk electrode in the presence of organic additive. J. Electrochem. Soc. **144**(5), 1560 (1997). https://doi.org/10.1149/1.1837641

20. Bai, A., Hu, C.C.: Effects of electroplating variables on the composition and morphology of nickel–cobalt deposits plated through means of cyclic voltammetry. Electrochim. Acta **47**(21), 3447–3456 (2002). https://doi.org/10.1016/S0013-4686(02)00281-5

21. Oriňáková, R., Oriňák, A., Vering, G., Talian, I., Smith, R.M., Arlinghaus, H.F.: Influence of pH on the electrolytic deposition of Ni–Co films. Thin Solid Films **516**(10), 3045–3050 (2008). https://doi.org/10.1016/j.tsf.2007.12.081

22. Tsay, P., Hu, C.C.: Non-anomalous codeposition of iron-nickel alloys using pulse-reverse electroplating through means of experimental strategies. J. Electrochem. Soc. **149**(10), C492 (2002). https://doi.org/10.1149/1.1504718